Biosensors and Bioelectronics 38 (2012) 43–49

Contents lists available at SciVerse ScienceDirect

Biosensors and Bioelectronics

journal homepage: www.elsevier.com/locate/bios

Highly sensitive visible light activated photoelectrochemical biosensing of organophosphate pesticide using biofunctional crossed bismuth oxyiodide flake arrays

Jingming Gong *, Xiaoqing Wang, Xue Li, Kewei Wang

Key Laboratory of Pesticide and Chemical Biology of Ministry of Education, College of Chemistry, Central China Normal University, Wuhan 430079, PR China

ARTICLE INFO

Article history:
Received 20 March 2012
Received in revised form
26 April 2012
Accepted 27 April 2012
Available online 11 May 2012

Keywords:
Organophosphate pesticides
BiOI flake arrays
Photoelectrochemical detection
Biosensor
Acetylcholinesterase

ABSTRACT

A new, highly sensitive and selective biosensor for the photoelectrochemical (PEC) detection of organophosphate pesticides (OPs) has been developed, whereby newly synthesized crossed bismuth oxyiodide (BiOI) nanoflake arrays (BiOINFs) are fabricated as a photoactive electrode via a successive ionic layer adsorption and reaction (SILAR) approach. The smart integration of BiOINFs with biomolecules acetylcholinesterase (AChE) yields a novel AChE–BiOINFs hybrid, constructing a three-dimensional (3D) porous network biosensing platform. The composition and surface structure of the sensor were carefully characterized by X-ray diffraction (XRD), scanning electron microscopy (SEM), and various electrochemical techniques. Such interlaced network architectures, providing better mass transport and allowing more AChE loading per unit area, as well as the intrinsically strong visible light-harvesting effect from BiOI, greatly facilitate the PEC responses. On the basis of the effect of OPs on the photocurrent of AChE–BiOINFs/ITO, a highly sensitive visible light-activated photoelectrochemical biosensor was developed for biosensing OPs. The conditions for OPs detection were optimized by using methyl parathion (MP) as a model OP compound. Under the optimized experimental conditions, our results show that such a newly designed AChE–BiOINFs/ITO photoactive electrode provides remarkably improved sensitivity and selectivity for the biosensing of OPs. The detection limit was found to be as low as about 0.04 ng mL^{-1} ($S/N=3$). Toward the goal for practical applications, the resulting sensor was further evaluated by monitoring MP in spiked vegetable samples, showing fine applicability for the detection of MP in real samples.

1. Introduction

Organophosphates pesticides (OPs) have been widely used as pesticides in agriculture for pest control and as nerve agents in military and terrorist attacks. However, because of OPs persistence, bioaccumulation, and high toxicity both in animals and in humans, serious concerns regarding the healthiness, environment and food safety are being raised (Giordano and Collins, 2007; Watson et al., 2006; Arduini et al., 2006; Li et al., 2007). For the sake of human health protection and environmental control, the detection of trace level of OPs has become increasingly important.

Well established methods over the past decades include gas/liquid chromatography or mass spectroscopy (Chen and Huang, 2006; Rotiroti et al., 2005; Leandro et al., 2006). These methods often require complicated pretreatment steps, expensive labor resources, and are not applicable for in situ rapid analysis. Compared with the conventional methods, newly developed photoelectrochemical (PEC) detection is of great interest for its rapid and high-throughput biological assay (Brown et al., 1992; Cooper et al., 1998; Tokudome et al., 2005; Chen et al., 2010). Owing to the efficient separation of excitation source (light) and detection signal (current), some undesired background signals could be reduced greatly, thus leading to high sensitivity achieved (Cooper et al., 1998). On the other hand, advantageously inherited from the electrochemical technique, the use of an electronic readout makes the instrument simpler, cheaper, and easier to miniaturize than that of conventional optical methods. As a result of its remarkable sensitivity, inherent miniaturization, portability and easy integration, PEC analysis is becoming a promising analytical technique (Cooper et al., 1998; Zhu et al., 2009; Zhao et al., 2011; Kang et al., 2010; Tu et al., 2010). Currently, the exploration of photoactive materials-based sensing platform is a considerably critical issue, directly related to the stability of biological recognition element and the final sensing performance. Some metal oxide semiconductor nanoparticles such as ZnO, ZrO_2, and TiO_2 have been used as significant PEC materials. Among

* Corresponding author. Tel: +86 27 6786 7535.
E-mail address: jmgong@mail.ccnu.edu.cn (J. Gong).

0956-5663/$ - see front matter Crown Copyright © 2012 Published by Elsevier B.V. All rights reserved.
http://dx.doi.org/10.1016/j.bios.2012.04.040

them, TiO_2 has been extensively investigated for various PEC applications because of its strong oxidizing power, non-toxicity, low cost, and biological and chemical inertness (Zhao et al., 2004a,b; Zhou et al., 2005; Wen et al., 2010). However, TiO_2 is effective only under ultraviolet irradiation ($\lambda < 400$ nm) due to its wide band gap, which may cause the deactivation of biomolecules (Wen et al., 2010; Zou et al., 2001). Furthermore, the strong oxidizing power of the photogenerated holes upon illumination may also cause destructive effects for biomolecules. To address this, further modification of TiO_2 is essential for the PEC application. For instance, nanotubular TiO_2 structures (TNs) (Chen et al., 2010), Au-doped TNs (Zhu et al., 2009), CdS-precipitated TNs (Zhao et al., 2011), multiple hybrid $CdSe_xTe_{1-x}$/TNs (Kang et al., 2010), and Porphyrin-functionalized TNs (Tu et al., 2010) have been exploited as highly efficient photoactive materials. These materials exhibit remarkable superiorities on the PEC sensing applications, with the enhanced absorption ability toward visible light and increased lifetime of the charge carriers. Despite these outstanding achievements, to meet the fast-developing detection requirements (e.g. simple operations, economical expense, high sensitivity, and portable instruments), it is still a great challenge to exploit a high-performance photoactive material, e.g. shifting the threshold of the photoresponse into the visible, for PEC biosensing.

Bismuth oxyhalides (BiOX, X=F, Cl, Br, and I), novel ternary oxide semiconductor, are recently becoming increasingly important in photochemistry field. They possess unique layered structures with the internal static electric field perpendicular to each layer, which can induce the effective separation of photo-generated electron–hole pairs, and therefore recognized as the light harvesting materials (Song et al., 2010; Ma et al., 2010; Zhang et al., 2008a,b; Xiao and Zhang, 2011). Among them, owing to the smallest band gap (~1.8 eV) and strong absorption in the visible light region (the absorption edge is ~680 nm), BiOI has drawn much attention in photocatalysis, exhibiting excellent photocatalytic performance under sunlight irradiation (Zhang et al., 2008a,b; Xiao and Zhang, 2010; Chang et al., 2009). Recently, our group developed a successive ionic layer adsorption and reaction (SILAR) approach to fabricate crossed BiOI nanoflake arrays (BiOINFs) and further explored its applications on solar cell (Zhao et al., 2009; Wang et al., 2010a,b). The three-dimensional interlaced network of BiOINFs with large surface area should be a good immobilization matrix for biomolecules. Inspired by this idea, here we present for the first time, the novel applications of biofunctional crossed BiOINFs for PEC biosensing of OPs under visible light irradiation.

The first smart integration of BiOINFs with biomolecules acetylcholinesterase (AChE) yields a novel AChE–BiOINFs hybrid as a photoactive electrode. Upon visible light irradiation, the biofunctional photocathode (AChE–BiOINFs/ITO) could produce cathodic photocurrent, which would be significantly influenced by the addition of OPs, due to AChE inhibition induced. On the basis of the effect of OPs on the photocurrent of AChE–BiOINFs/ITO, a new rapid and valid visible light-activated photoelectrochemical approach was developed for biosensing OPs. The new strategy, via constructing the novel biofunctional AChE–BiOINFs photoactive sensing platform, effectively avoids the complicated fabrication process of TNs and the tedious integration procedures with other exotic units, significantly saving cost and time. Furthermore, it would largely reduce the destructive effects of UV light and the photogenerated holes of illuminated TiO_2 to biomolecules. The as-formed BiOINFs-based composite combines the intrinsically excellent properties of BiOI enabled by visible light with the unique nanostructure, *i.e.* interlaced network of BiOI nanoflake arrays (an advantageous platform for the immobilization of AChE). It is expected that such a nanostructured composite of AChE–BiOINFs would dramatically facilitate the sensitive determination of OPs. To the best of our knowledge, this is the first report on utilizing biofunctional crossed BiOINFs for photoelectrochemical biosensing of OPs.

2. Experiments

2.1. Reagents

Acetylthiocholine chloride (ATCl) and AChE (TypeC3389, 500 U mg^{-1} from electric eel) were purchased from Sigma-Aldrich (St. Louis, USA) and used as received. The ITO glass was purchased from NSG, Japan. Methyl parathion (MP) was obtained from Treechem Co (Shanghai, China). $Bi(NO_3)_3 \cdot 5H_2O$, KI (AR, ≥98.5%) and other reagents of analytical reagent grade were obtained from commercial sources and used as received. Ultrapure water (resistivity ≥ 18 MΩ) was used during the experiment process. Measurements were performed in 0.1 M phosphate buffer solution (PBS) prepared with $KHPO_4$ and K_2HPO_4. The whole experiments were carried out at room temperature.

2.2. Apparatus

The compositions of samples were measured by powder X-ray diffraction (XRD) on a Bruker D8 Advance X-ray diffractometer with Cu Kα radiation (λ=1.54178 Å). The morphologies of the films were characterized by scanning electron microscopy (SEM, JSM 5600). Electrochemical and photoelectrochemical measurements were performed on a CHI 660D electrochemical workstation (CHI, USA) with a conventional three electrode system comprising platinum wire as auxiliary electrode, a standard Ag/AgCl in saturated KCl solution as the reference electrode, and the as-prepared crossed BiOINFs onto ITO electrode (labeled as BiOINFs/ITO) or AChE immobilized BiOINFs onto ITO electrode (labeled as AChE–BiOINFs/ITO) as the working electrode. A 500 W Xe lamp (Shanghai LanSheng Electronic Co., Ltd., Shanghai, China) equipped with a monochromator was used as the irradiation source (λ=420 nm). Electrochemical impedance spectra (EIS) were measured in the frequency range from 0.1 Hz to 100 kHz with a signal amplitude of 5 mV at CHI 660D. During the electrochemical measurements, the surface area of the working electrode was ca. 1.8 cm^2.

2.3. Electrode preparation of BiOINFs/ITO and AChE–BiOINFs/ITO

Prior to the preparation of AChE–BiOINFs/ITO electrodes, the basal ITO substrates were cleaned by ultrasonication in distilled water and ethanol, subsequently. The crossed BiOI nanoflake arrays modified ITO (BiOINFs/ITO) were prepared according to the previous report, via a SILAR approach (Wang et al., 2010a,b). Briefly, 5 mM $Bi(NO_3)_3 \cdot 5H_2O$ and 5 mM KI solutions were prepared in separate glass beakers with ultrapure water. The pretreated ITO was first immersed in the $Bi(NO_3)_3$ solution, followed by the subsequent washing step, and then immersed in KI solution. The immersion time for each solution and washing process, taken place in separated beaker, was set ~10 s. After certain cycles of SILAR, the resulting BiOINFs/ITO was dried at room temperature. AChE enzyme immobilization was achieved by immersing the obtained BiOINFs/ITO in 5 mM phosphate buffer (pH 7.0) containing 6 mU mL^{-1} of AChE for over 6 h. Then, the AChE–BiOINFs/ITO electrode was rinsed in phosphate buffer for 20 min to remove the nonimmobilized protein. The resulting AChE–BiOINFs/ITO electrode was stored in 5 mM phosphate buffer at pH 7.0 and 4 °C for use.

2.4. Photoelectrochemical biosensing under visible light illumination

For the measurements of methyl parathion (MP) as the model of OPs, the obtained AChE–BiOINFs/ITO electrode was first immersed in PBS solution containing different concentrations of standard MP for 10 min, and then transferred to the half arc electrochemical cell of 80.0 mL (pH 7.0) PBS containing 0.8 mM acetylthiocholine chloride (ATCl), an enzyme substrate, to study the photoelectrochemical response. For comparison, the PEC responses were also recorded by immersing the AChE–BiOINFs/ITO electrode in a solution of 0.8 mM ATCl for ~10 min in the absence of MP. The inhibition of methyl parathion was calculated as follows:

$$\text{inhibition}(\%) = \frac{i_{P,\ \text{control}} - i_{P,\ \text{exp}}}{i_{P,\ \text{control}}} 100$$

where $i_{P,\ \text{control}}$ and $i_{P,\ \text{exp}}$ is the photocurrent of ATCl on the AChE–BiOINFs/ITO electrode, in the absence and presence of MP inhibition, respectively.

3. Results and discussion

3.1. Characterization of the modified photoactive electrodes

Fig. 1A shows the XRD pattern of the prepared BiOI by a successive ionic layer adsorption and reaction (SILAR) after 30 cycles. The characteristic diffraction peaks observed at about $2\theta = 9.86^\circ$, 19.4°, 24.4°, 29.8°, 31.9°, 33.3°, 39.3°, 45.6°, 51.5°, 55.5°, and 66.4° are indexed to a typical tetragonal crystal structure of BiOI (JCPDS no. 73-2062). It indicates that the tetragonal structured BiOI onto the ITO substrate has been successfully prepared via a SILAR approach, agreeing well with the previous report (Wang et al., 2010a,b). The typical SEM images of the prepared BiOI and modified BiOI onto ITO substrate, were shown in Fig. 1(B) and (C), respectively. Free-standing crossed nanoflakes, obtained through 30 SILAR cycles, were observed to be uniformly distributed over the whole ITO substrate (Fig. 1B). A high-magnification SEM image (inset of Fig. 1B) further shows that each nanoflake has a lateral dimension in the micrometer size and an average thickness of ~10 nm. Generally, the porous nanostructured substrate is highly desirable for the immobilization of protein, directly affecting the final performance of biosensors. Such interlaced network structures of BiOINFs construct an advantageous immobilization matrix for biomolecules. With the immobilization of AChE, it was found that the morphology of AChE–BiOINFs (Fig. 1C) is very similar to that of BiOINFs, indicating that the structural morphologies of BiOI remained unchanged after the immobilization.

The immobilization of AChE on the BiOINFs is further evidenced by the electrochemical impedance spectrum (EIS) measurements, which is an effective tool for characterizing the interface properties of electrodes. Fig. 1(D) shows the typical EIS for the electrodes of bare ITO, BiOINFs/ITO, and AChE–BiOINFs/ITO. It can be seen that EIS of the bare ITO is composed of a semicircle and a straight line featuring a diffusion-limiting step of the $Fe(CN)_6^{4-/3-}$ processes (curve a). With the formation of the crossed BiOINFs onto ITO, the semicircle increases significantly as compared to the bare ITO, suggesting the hindrance effect to the interfacial charge transfer, caused by the formation of the BiOI insulating thin film on the electrode surface (curve b). After the immobilization of AChE onto BiOINFs/ITO, the semicircles further increased distinctively (curve c). Obviously, the nonconductive properties of proteins would obstruct electron transfer and mass transport of the electrochemical probe, resulting in the increased resistance. The EIS measurements further demonstrated the successful preparation of biofunctional AChE-immobilized BiOINFs.

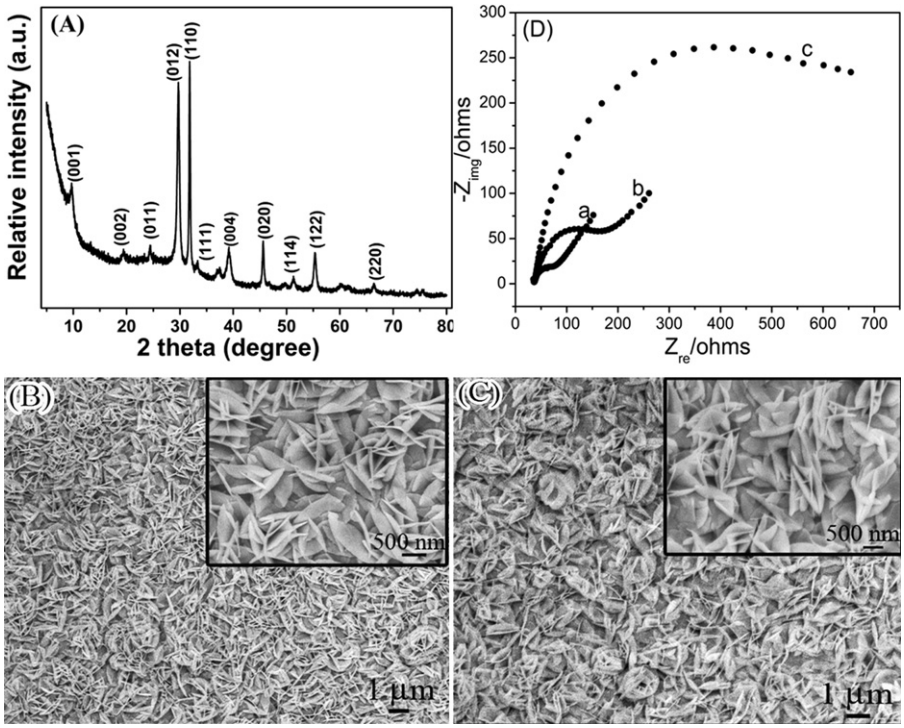

Fig. 1. (A) XRD pattern of the as-prepared composite film of BiOINFs on the ITO substrate (BiOINFs/ITO) via a SILAR approach (total 30 cycles); typical SEM images: (B) the as-prepared BiOINFs; (C) AChE–BiOINFs composite film on the ITO substrate. Inset: corresponding magnified SEM image; (D) electrochemical impedance spectra of (a) ITO foil, (b) BiOINFs/ITO, and (c) AChE–BiOINFs/ITO, which were measured in 0.1 M phosphate buffer solution containing 2.5 mM $K_3[Fe(CN)_6]/K_4[Fe(CN)_6]$ (1:1) mixture. The applied frequency was from 0.1 Hz to 100 kHz. The BiOINFs/ITO was obtained by 30 SILAR cycles.

3.2. Photocurrent behaviors of the prepared electrodes

To investigate the visible light photoinduced behavior of the generated photocurrent, the photocurrent responses of the ITO, BiOINFs/ITO, and AChE–BiOINFs/ITO electrodes illuminated are shown in Fig. 2(A). When the light was regularly switched on and off, a series of almost identical PEC responses could be obtained. As expected, upon the visible light irradiation, the BiOI showed obvious photocurrent response (Fig. 2A curve b). In comparison to the BiOINFs/ITO electrode, with the introduction of AChE onto BiOINFs/ITO, the photocurrent of AChE–BiOINFs/ITO was slightly enhanced (Fig. 2A curve c), probably due to the light-harvesting effect of AChE toward visible light as well as the permission of electron or energy migration between AChE and BiOINFs. It was similar to the photoinduced behavior of HRP–TNs (Chen et al., 2010). Interestingly, the further addition of acetylthiocholine chloride (ATCl), an enzyme substrate, results in a significantly enhanced photocurrent in the AChE–BiOINFs/ITO hybrid system (Fig. 2A curve d). It could be explained as follows: when this system is exposed to a solution containing ATCl, the immobilized AChE can hydrolyze ATCl into acetate and thiocholine. Upon irradiation, the latter product of thiocholine acts as a sacrificial electron donor to scavenge the holes and improves the efficiency of charge separation, leading to a prominent increase in the photocurrent. Control experiments, which were performed with the BiOINFs/ITO incubated in ATCl without AChE modification, showed no enhancement of the photocurrent. These further demonstrated that the crossed BiOINFs provide an excellent matrix for AChE immobilization, and the adsorbed AChE effectively retained its bioactivities. Because of the fairly high acute toxicity of OPs toward AChE, the presence of OPs induces the irreversible inhibition action on AChE, accompanied with the reduced the enzymatic activity to the substrate (ATCl). Thus, with the successive addition of methyl parathion (MP, as the model of OPs), the photocurrent in AChE–BiOINFs/ITO would decrease successively (Fig. 2B curve a–d), which hereby can be used as an indicator for quantitative measurement of OPs. Due to the notable change in photoelectrochemical signal of the AChE–BiOINFs/ITO, the intriguing applications of biofunctional crossed BiOINFs for photoelectrochemical biosensing of OPs under visible light irradiation could be established (illustrated in Scheme 1).

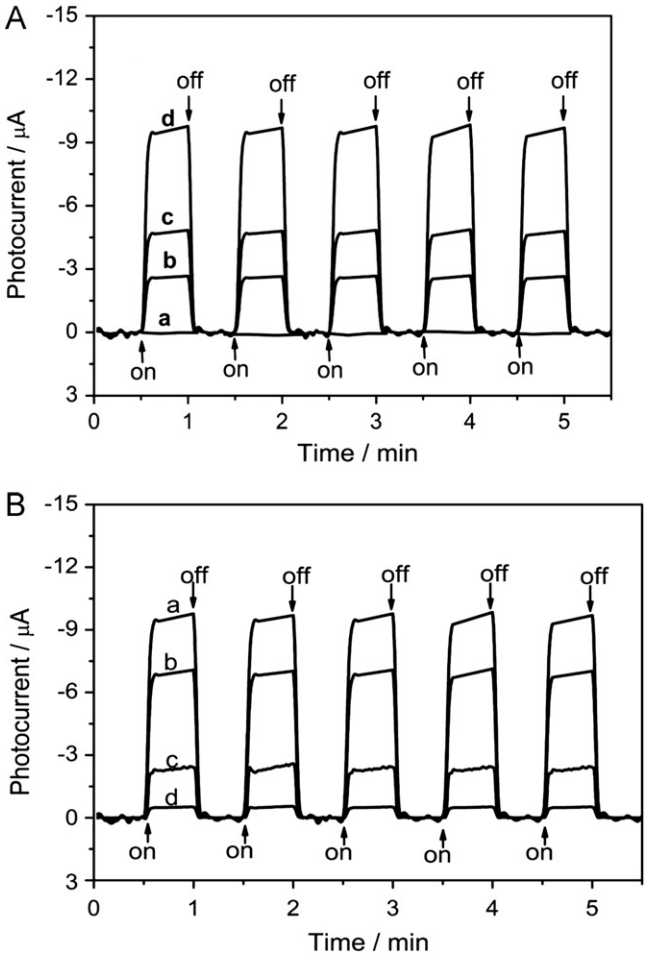

Fig. 2. (A)The photocurrent responses of (a) ITO, (b) BiOINFs/ITO, and (c) AChE–BiOINFs/ITO in the supporting electrolyte of 0.1 M pH 7.0 PBS, and (d) AChE–BiOINFs/ITO in the presence of 0.1 M pH 7.0 PBS containing 0.8 mM ATCl; (B) photocurrent responses of AChE–BiOINFs/ITO in the presence of 0.1 M pH 7.0 PBS containing 0.8 mM ATCl after incubation in (a) 0, (b) 10.0, (c) 100, and (d) 1000 ng mL^{-1} methyl parathion solution, subsequently, for 12 min with on–off illumination under visible light.

3.3. Optimization for the photoelectrochemical responses at AChE–BiOINFs/ITO

To get high-performance visible light-activated photoelectrochemical responses of AChE–BiOINFs/ITO, we further optimized the experimental parameters. As well known, the intrinsic properties of materials as well as their shape, size and structures have great influence on the photoconversion efficiency of photoactive materials. As shown in Fig. 3A, the photocurrent of BiOI rises at first up to 30 cycles and then decreases upon increasing the SILAR cycles. It is likely related to the nanostructural platform of BiOI on the electrode, since the numbers of cycles of SILAR directly influence the crystallization and morphology of the obtained BiOI (Wang et al., 2010a,b). Better crystallization could be obtained with more SILAR cycles, *i.e.* 30 cycles here. With SILAR cycles increased up to 30 cycles, the enhanced surface area from the crossed-nanoflake structures as well as good crystallization, guarantees the high photocurrent obtained. While the SILAR cycles were further increased, the nanostructure of BiOI would continuously evolve. Some aggregated nanostructures were produced (Wang et al., 2010a,b), resulting in the decreased PEC performance. Thus, the condition of 30 SILAR cycles is optimal.

The concentration of ATCl was one of the most influential parameters. When the concentration of ATCl was too low, the peak current generated by enzyme electrode was so small that

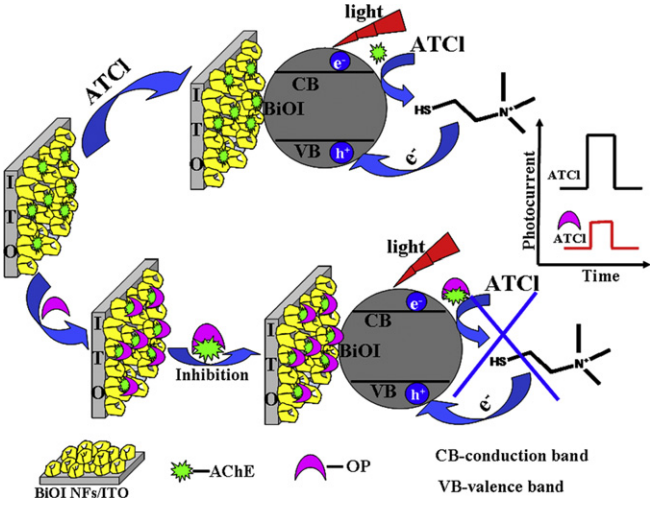

Scheme 1. Schematic illustration for the principle of photoelectrochemical determination of OP compound using AChE–BiOINFs/ITO.

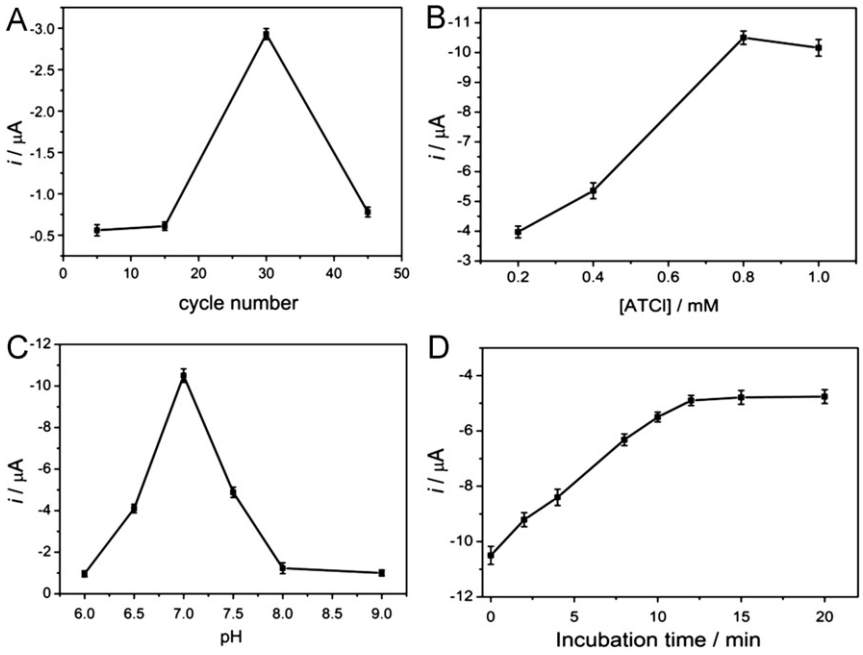

Fig. 3. Effects of (A) the cycle number of SILAR on the photocurrent responses of BiOINFs/ITO in the electrolyte of 0.1 M pH 7.0 PBS, (B) the concentration of ATCl, (C) the solution pH of 0.1 M PBS in the presence of 0.8 mM ATCl, and (D) the immersion time of 40 ng mL^{-1} MP on the photocurrent responses of AChE–BiOINFs/ITO. Supporting electrolyte: 0.1 M PBS (pH 7.0, unless specified). The data obtained with on–off illumination under visible light (λ=420 nm). Error bars indicate the standard deviation of five repeated measurements.

the determination of MP is hardly feasible. However, too high substrate concentration would cause all the active centers of AChE being occupied by the substrate and insensible to the inhibitor. The concentration of 0.8 mM ATCl is an optimized value (shown in Fig. 3B).

The bioactivity of the immobilized AChE depended on the solution pH. Fig. 3(C) shows the variations of the photocurrent at AChE–BiOINFs/ITO with the solution pH. Considering the stability of the supporting skeleton of BiOI, we start from the initial pH 6.0. Obviously, the maximum peak current was obtained at pH 7.0 in the pH range from 6.0 to 9.0. Therefore, pH 7.0 was used in the detection solution.

Inhibition time is another influential parameter in pesticide analysis. With an increase of immersion time in the MP solution, the photocurrent of ATCl on the AChE–BiOINFs/ITO was decreased greatly. As shown in Fig. 3(D), MP displayed an increasing inhibition on AChE with the immersion time increased. When the immersion time was longer than 12 min, the curve tended to a stable value, indicating the binding interactions with active target groups in the enzyme reached saturation. This change tendency of the photocurrent reflects an alteration of enzymatic activity, in turn resulting in the change of the interactions with its substrate. Notably, the maximum value of inhibition of MP was not 100%, which might be attributed to the binding equilibrium between pesticide and binding sites in the enzyme.

3.4. Analytical performance for visible light-activated photoelectrochemical biosensing of MP

The degree of photocurrent response of AChE–BiOINFs/ITO upon visible light irradiation was found to be dependent on the concentration of MP in the immersion solution, thus forming the PEC biosensing basis for real-time detection. Fig. 4A depicts the time-based photocurrent response of AChE–BiOINFs/ITO immersed in different concentrations of MP upon the visible light irradiation. Clearly, with increase in the concentration of MP in the immersion solution, the produced photocurrent at AChE–BiOINFs/ITO decreased successively. Under the optimized experimental conditions, as shown in Fig. 4B, the MP inhibition to AChE–BiOINFs/GCE was proportional to its concentration in two ranges, from 0.001 to 0.08 μg $mL^{-}1$ and 0.3 to 1.0 μg $mL^{-}1$. The linearization equations were inhibition (%)=656.9 c+27.91 (%), and inhibition (%)=12.31 c+82.07 (%), with the correlation coefficients of 0.9964 and 0.9985, respectively (inset of Fig. 4B). The detection limit was calculated to be about 0.04 ng $mL^{-}1$. The detection limit obtained is significantly lower than that reported so far with an enzyme-based inhibitor electrochemical sensor (Kok and Hasirci, 2004; Wang et al., 2010a,b; Gong et al., 2009a,b), also lower than those using stripping analysis (Liu and Lin, 2005; Gong et al., 2009a,b, 2011), indicating that the proposed biofunctional AChE–BiOINFs composite film is remarkably reliable for the determination of OPs. The higher sensitivity of the AChE–BiOINFs/ITO electrode could be attributed to the porous architecture of the AChE–BiOINFs film that provides better mass transport, and allows more AChE loading per unit area, as well as the intrinsic ultrahigh sensitivity from the PEC analytical system (Zhu et al., 2009).

To investigate the reproducibility of the AChE–BiOINFs/ITO electrode, five enzyme electrodes made by the same procedures independently showed a relative standard deviation of 3.6% for the photocurrent measurements of 0.04 μg mL^{-1} MP, indicating an acceptable reproducibility. The stability of the enzyme electrode could be maintained by being stored at 4 °C in dry condition. No obvious decrease in the response of ATCl was observed in the first 10-day storage. After a 30-day storage period, the sensor retained 92% of its initial current response. The interferences from the other electroactive nitrophenyl derivatives such as nitroaniline, trinitrotoluene (TNT), nitrophenol, nitrobenzene and other oxygen-containing inorganic ions (NO_3^-, SO_4^{2-} and PO_4^{3-}) were investigated. No obvious inhibition behavior can be observed with the peak currents of ATCl varied slightly (Fig. S1). While in the presence of other OPs instead of MP, such as paraoxon, rogor, and chlorpyrifo, etc., the obvious inhibition behavior can also be observed (Fig. S2). This implies that the proposed applications

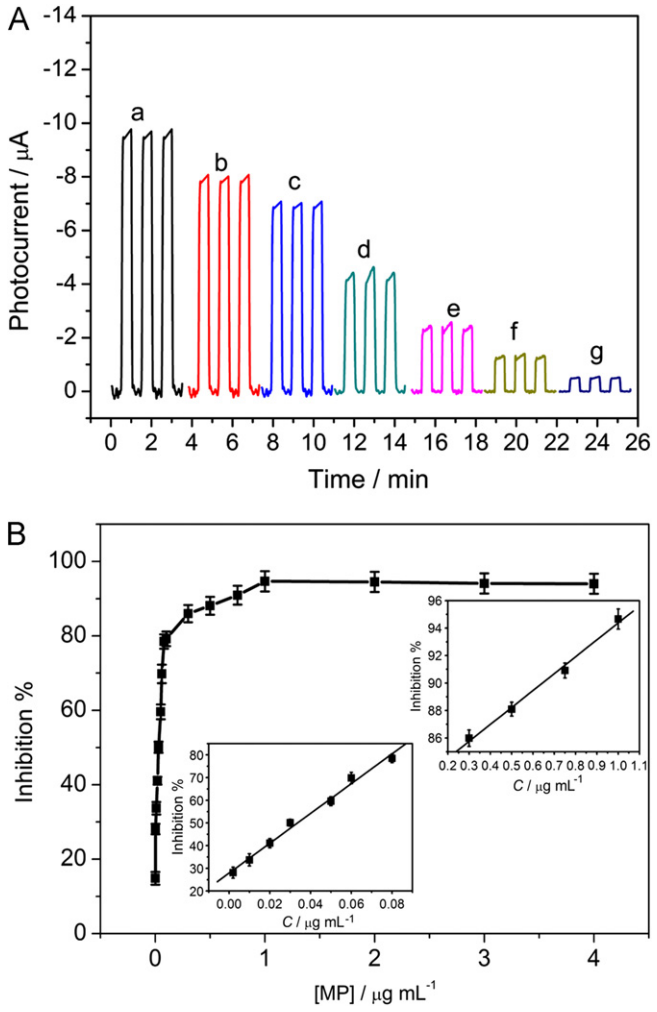

Fig. 4. Calibration curves for the photoelectrochemical determination of MP at AChE–BiOINFs/ITO in the supporting electrolyte of 0.1 M pH 7.0 PBS containing 0.8 mM ATCl. Inset: linear relationships between peak currents and MP concentrations.

of biofunctional BiOINFs for photoelectrochemical biosensing and the total amount of OPs could be established under visible light irradiation. In other words, the photoelectrochemical biosensor has an excellent specificity for the detection of OPs.

3.5. Analysis of the real samples and the reactivation of AChE–BiOINFs/ITO

To further demonstrate the practicality of the present electrode, it was evaluated by processing real samples. We performed the recovery tests by adding different amounts of MP into real samples (e.g. garlic, apple and cabbage). Results are summarized in Table 1. The recoveries of the spiked MP are from 96.0% to 104.1%. The original MP concentration in the cabbage sample was tested to be 0.0384 mg kg^{-1}, well below the guideline value of the individual pesticides in food of plant origin (0.05 mg kg^{-1}) set by the European Union (EEC, 1980). The accuracy of the method was also assessed by comparing the electrochemical results with those obtained by HPLC. The real sample of cabbage was analyzed using both methods. The original MP concentration in the cabbage sample was tested electrochemically to be 7.67 ± 0.01 ng mL^{-1} ($\sim$0.0384 mg kg^{-1}), and while a value of 8.80 ± 0.01 ng mL^{-1} was obtained by HPLC, showing a difference of 12.8%. The results further indicated that the proposed method was highly accurate, precise and reproducible. It can be used for direct analysis of relevant real samples.

Table 1
Photoelectrochemical detection of methyl parathion in real samples using the proposed method ($n=5$).

Sample	Concentration		RSD (%)	Recovery (%)
	Taken (ng mL^{-1})	Found (ng mL^{-1})		
Garlic 1	8.00	8.23	2.00	102.8
Garlic 2	15.00	15.37	1.20	102.4
Garlic 3	25.00	26.06	1.40	104.1
Garlic 4	35.00	33.94	1.10	97.0
Cabbage 1	0.00	7.67	3.00	
Cabbage 2	15.00	21.87	1.20	96.5
Cabbage 3	25.00	32.06	2.40	98.1
Cabbage 4	35.00	43.94	1.10	103.0
Apple 1	0.00	6.83	3.50	
Apple 2	8.00	15.07	2.20	101.6
Apple 3	25.00	30.56	1.13	96.0
Apple 4	35.00	41.94	1.40	100.2

Repeatability of the proposed sensor is very important for recycling utilizations. The AChE inhibited irreversibly by OPs can be completely reactivated by use of nucleophilic compounds such as pralidoxime iodide. It was observed that the AChE modified electrode inhibited by MP could resume 95% original activity after immersing in 6.0 mM pralidoxime iodide (Fig. S3a). With increase in the reactivation time, the reactivation efficiency R% increased and reached stability at $\sim$10 min (Fig. S3b). Based on this reactivation procedure, the proposed biosensor could be used repeatedly with an acceptable recycle performance.

4. Conclusions

A novel photoelectrochemical biosensing platform was developed using newly synthesized crossed BiOI nanoflake arrays, which were prepared by a SILAR approach. The first smart integration of BiOINFs with biomolecules AChE yields a novel AChE–BiOINFs hybrid as a photoactive electrode. Such interlaced network architectures, providing better mass transport and allowing more AChE loading per unit area, as well as the intrinsically strong visible light harvesting effect from BiOI, greatly facilitate the PEC responses. Upon visible light irradiation, the biofunctional AChE–BiOINFs/ITO electrode showed obvious photocurrent responses, which would be significantly influenced by the addition of OPs. On the basis of the effect of OPs on the photocurrent of AChE–BiOINFs/ITO, a new rapid and valid visible light activated PEC approach was developed for biosensing OPs. The resulting biosensor showed good sensitivity, reproducibility, ideal stability and fine applicability for the detection of methyl parathion in real samples. We believe that this work may open a new avenue for the application of crossed BiOI nanoflake arrays on visible light activated photoelectrochemical biosensing.

Acknowledgments

This work was supported by the Natural Science Foundation of China (21175053, 91023010), the Program for Chenguang Young Scientist for Wuhan (201271031412) and Self-determined Research Funds of CCNU from the Colleges' Basic Research and Operation of MOE (CCNU10A01006).

Appendix A. Supporting information

Supplementary data associated with this article can be found in the online version at http://dx.doi.org/10.1016/j.bios.2012.04.040.

References

Arduini, F., Ricci, F., Tuta, C.S., Moscone, D., Amine, A., Palleschi, G., 2006. Analytica Chimica Acta 580, 155–162.

Brown, G.N., Birks, J.W., Koval, C.A., 1992. Analytical Chemistry 64, 427–434.

Chang, X.F., Huang, J., Tan, Q.Y., Wang, M., Ji, G.B., Deng, S.B., Yu, G., 2009. Catalysis Communications 10, 1957–1961.

Chen, D., Zhang, H., Li, X., Li, J.H., 2010. Analytical Chemistry 82, 2253–2261.

Chen, P.S., Huang, S.D., 2006. Talanta 69, 669–675.

Cooper, J.A., Wu, M., Compton, R.G., 1998. Analytical Chemistry 70, 2922–2927.

EEC, 1980. Drinking Water Guideline, EEC. Brussels, Belgium, 80/779/EEC No. L229/11-29.

Giordano, B.C., Collins, G.E., 2007. Current Organic Chemistry 11, 255–256.

Gong, J.M., Liu, T., Song, D.D., Zhang, X.B., Zhang, L.Z., 2009a. Electrochemistry Communications 11, 1873–1876.

Gong, J.M., Miao, X.J., Zhou, T., Zhang, L.Z., 2011. Talanta 85, 1344–1349.

Gong, J.M., Wang, L.Y., Song, D.D., Zhu, X.L., Zhang, L.Z., 2009b. Biosensors and Bioelectronics 25, 493–496.

Kang, Q., Yang, L.X., Chen, Y.F., Luo, S.L., Wen, L.F., Cai, Q.Y., Yao, S.Z., 2010. Analytical Chemistry 82, 9749–9754.

Kok, F.N., Hasirci, V., 2004. Biosensors and Bioelectronics 19, 661–665.

Leandro, C.C., Hancock, P., Fussell, R.J., Keely, B.J., 2006. Journal of Chromatography A 1103, 94–101.

Li, B.X., He, Y.Z., Xu, C.L., 2007. Talanta 72, 223–230.

Liu, G.D., Lin, Y.H., 2005. Analytical Chemistry 77, 5894–5901.

Ma, J.M., Liu, X.D., Lian, J.B., Duan, X.C., Zheng, W.J., 2010. Crystal Growth and Design 10, 2522–2527.

Rotiroti, L., Stefano, L.D., Rendina, I., Moretti, L., 2005. Biosensors and Bioelectronics 20, 2136–2139.

Song, J.M., Mao, C.J., Niu, H.L., Shen, Y.H., Zhang, S.Y., 2010. CrystEngComm 12, 3875–3881.

Tokudome, H., Yamada, Y., Sonezaki, S., Ishikawa, H., Bekki, M., Kanehira, K., Miyauchi, M., 2005. Applied Physics Letters 87, 213901–213903.

Tu, W.W., Dong, Y.T., Lei, J.P., Ju, H.X., 2010. Analytical Chemistry 82, 8711–8716.

Wang, K.W., Jia, F.L., Zheng, Z., Zhang, L.Z., 2010a. Electrochemistry Communications 12, 1764–1767.

Wang, Y.Z., Qiu, H.X., Hu, S.Q., Xu, J.H., 2010b. Sensors and Actuators B 147, 587–592.

Watson, A., Opresko, D., Young, R., Hauschild, V., 2006. Journal of Toxicology and Environmental Health, Part B 9, 173–263.

Wen, D., Guo, S.J., Wang, Y.Z., Dong, S.J., 2010. Langmuir 26, 11401–11406.

Xiao, X., Zhang, W.D., 2011. RSC Advances 1, 1099–1105.

Xiao, X., Zhang, W., 2010. Journal of Materials Chemistry 20, 5866–5870.

Zhang, J., Shi, F.J., Lin, J., Chen, D.F., Gao, J.M., Huang, Z.X., Ding, X.X., Tang, C.C., 2008a. Chemistry of Materials 20, 2937–2941.

Zhang, X., Ai, Z.H., Jia, F.L., Zhang, L.Z., 2008b. Journal of Physical Chemistry C 112, 747.

Zhao, H.J., Jiang, D.L., Zhang, S.Q., Catterall, K., John, R., 2004a. Analytical Chemistry 76, 155–160.

Zhao, K., Zhang, X., Zhang, L.Z., 2009. Electrochemistry Communications 11, 612–615.

Zhao, W.W., Yu, P.P., Xu, J.J., Chen, H.Y., 2011. Electrochemistry Communications 13, 495–497.

Zhao, H.J., Jiang, D.L., Zhang, S.Q., Catterall, K., John, R., 2004b. Analytical Chemistry 76, 155–160.

Zhou, H., Gan, X., Wang, J., Zhu, X.L., Li, G.X., 2005. Analytical Chemistry 77, 6102–6104.

Zhu, W., An, Y.R., Luo, X.M., Wang, F., Zheng, J.H., Tang, L.L., Wang, Q.J., Zhang, Z.H., Zhang, W., Jin, L.T., 2009. Chemical Communications 19, 2682–2684.

Zou, Z.G., Ye, J.H., Sayama, K., Arakawa, H., 2001. Nature 414, 625–627.